Journal of Molecular Modeling (2024) 30:127
https://doi.org/10.1007/s00894-024-05926-z

ORIGINAL PAPER

Molecular docking and molecular dynamics simulation decoding molecular mechanism of EDCs binding to hERRγ

Ying Sun[1] · Lin Chen[1] · Bing Zhao[1,2] · Ruige Wang[1]

Received: 17 October 2023 / Accepted: 3 April 2024 / Published online: 9 April 2024

Abstract

Context Human estrogen-related receptor γ (hERRγ) is a key protein involved in various endocrines and metabolic signaling. Numerous environmental endocrine-disrupting chemicals (EDCs) can impact related physiological activities through receptor signaling pathways. Focused on hERRγ with 4-isopropylphenol, bisphenol-F (BPF), and BP(2,2)(Un) complexes, we executed molecular docking and multiple molecular dynamics (MD) simulations along with molecular mechanics/Poisson-Boltzmann surface area (MM-PBSA) and solvation interaction energy (SIE) calculation to study the detailed dynamical structural characteristics and interactions between them. Molecular docking showed that hydrogen bonds and hydrophobic interactions were the prime interactions to keep the stability of BPF-hERRγ and hERRγ-BP(2,2)(Un) complexes. Through MD simulations, we observed that all complexes reach equilibrium during the initial 50 ns of simulation, but these three EDCs lead to local structure changes in hERRγ. Energy results further identified key residues L268, V313, L345, and F435 around the binding pockets through CH-π, π-π, and hydrogen bonds interactions play an important stabilizing role in the recognition with EDCs. And most noticeable of all, hydrophobic methoxide groups in BP(2,2)(Un) is useful for decreasing the binding ability between EDCs and hERRγ. These results may contribute to evaluate latent diseases associated with EDCs exposure at the micro level and find potential substitutes.

Method Autodock4.2 was used to conduct the molecular docking, sietraj program was performed to calculate the energy, and VMD software was used to visualize the structure. Amber18 was conducted to perform the MD simulation and other analyses.

Keywords Human estrogen-related receptor γ · Environmental endocrine-disrupting chemicals · Molecular docking · MD simulations · MM-PBSA SIE

Introduction

With the discharge substances and decomposition substances of pesticides, washing liquid, plastic industry, and so on, a large number of environmental endocrine-disrupting chemicals (EDCs) are produced in nature [1, 2]. EDCs possess hormonal and estrogen-like activity that are environmentally stable and not easily destroyed. So they can be enriched through the food chain in the ecological environment. Upon entering the human body, they can combine with the corresponding "receptors," resulting in changes in the biochemical reaction of the body, and potentially causing abnormal changes in the body and reproductive system [3–5]. For example, 4-isopropylphenol is a compound commonly used in antimicrobial and antifungal products for disinfection, sterilization, and preservation. Additionally, it is utilized as a food additive to keep food fresh and extend its shelf life. In the pharmaceutical field, it is also employed in the production of certain drugs, exhibiting specific pharmacological effects [6]. Besides, bisphenol F (BPF) is commonly used in industry as a raw material for manufacturing epoxy resins and other plastic products. Additionally, BPF is also utilized in coatings, sealants, adhesives, and other industrial products [7]. Due to the fact that 4-isopropylphenol and BPF belong to the group of phenols, it may potentially cause some health and environmental issues. Therefore, it

✉ Lin Chen
chenlin201308@163.com

✉ Ruige Wang
wangrg716@163.com

[1] College of Chemistry and Chemical Engineering, Qiqihar University, Qiqihar 161006, China

[2] Heilongjiang Provincial Key Laboratory of Surface Active Agent and Auxiliary, Qiqihar University, Qiqihar 161006, China

is of great significance to study these endocrine disruptors to find potential substitutes.

Human estrogen-related receptor γ (hERRγ) is an important nuclear receptor [8]. It is involved in regulating glucose and lipid metabolism pathways, influencing the differentiation and activation of brown adipocytes, as well as mitochondrial biogenesis and function. Abnormal activation or inhibition of hERRγ may lead to endocrine disruption, affecting the balance of the body's endocrine system and causing metabolic diseases such as obesity and diabetes [9]. Besides, hERRγ can also regulate the expression of various genes, affecting cell cycle regulation and the direction of cell differentiation. By interacting with other transcription factors and regulatory factors, hERRγ participates in a complex network regulating cell proliferation and differentiation. Aberrant hERRγ activity may lead to uncontrolled cell proliferation or abnormal cell differentiation, closely associated with diseases such as obesity and cancer [10]. hERRγ mainly including ligand independent activation function 1 (AF-1), DNA binding domain (DBD), and ligand binding domain (LBD) [11]. LBD contains another ligand-dependent transcriptional activation region, which presents a different configuration binding to different estrogens and determines which co-activators and co-inhibitors bind to transcription target gene. LBD is composed of two double-stranded antiparallel β-sheets (S1 and S2) and 12 α-helices (H1-H12) with a hydrophobic binding pocket of the EDCs. Most EDCs in the external environment can be located in this pocket, thereby interfering with downstream signaling pathways [12]. When its normal function is affected by EDCs such as 4-isopropylphenol and BPF, it can severely affect normal function of the body [13–16]. Experimental research revealed that 4-isopropylphenol and BPF have low binding capacity with hERRγ, with EC50 values of about 300 and 645 nM, respectively [12]. However, the specific details are currently unclear. Furthermore, lignin, as a renewable raw material, is a natural polymer that exists in plant cell walls. For example, renewable bisphenols derived from lignin, BP(2,2)(Un) is considered as the potential alternative of commercial bisphenols [17]. With its abundance of aromatic hydroxyl and methoxy groups, this compound is utilized in the production of bioplastics and bio-based chemicals, contributing to a decrease in reliance on petroleum resources and minimizing environmental impact. In addition, reports by molecular docking methods have shown that BP(2,2)(Un) has weak binding ability to ERα [17]. Nevertheless, the dynamic interactions between these three EDCs with hERRγ at the micro level have not yet been came to light. Therefore, in-depth study on the interaction mechanisms of hERRγ by these EDCs is crucial for deciphering the endocrine disrupting mechanisms of hERRγ, which contributes to comprehensively evaluate latent diseases associated with EDCs exposure.

In recent years, in silico approaches such as molecular docking and molecular dynamics (MD) simulation [18–23] have emerged as reliable tools for exploring the three-dimensional structure of protein complexes with small compounds, identifying key binding residues, evaluating interaction strength, conducting energy analysis, elucidating interaction mechanisms, understanding ligands binding with proteins pockets, and estimating the stability of the complexes. Hence, in our work, molecular docking and multiple MD simulations were executed to obtain the conformation of hERRγ-EDCs and to describe the dynamic and detailed interactions between them, which are difficult for experiment studies. We also performed molecular mechanics/Poisson-Boltzmann surface area (MM-PBSA) [24] plus solvation interaction energy (SIE) methods [25, 26] to investigate thoroughly the recognition mechanisms of hERRγ by these EDCs, including 4-isopropylphenol, BPF, and BP(2,2)(Un) (Fig. 1), and important residues distributions were also evaluated. The results could provide novel insights into estrogenic disruption effects of EDCs.

Methods

Molecular systems

Complexes coordinates of hERRγ-4-isopropylphenol were acquired from RCSB (PDB ID: 6I65) [12]. The binding site of 4-isopropylphenol to hERRγ was used as the active site for docking study. Initially, the EDC 4-isopropylphenol was redocked with the experimental protein hERRγ to verify the robustness of the docking procedure. Upon superimposing the experimental and docked complexes, it was observed that the conformation remained consistent across both structures (Fig. S1). Since there were no complexes of hERRγ with BPF and BP(2,2)(Un) were available, AutoDock software [27] was conducted to dock these two molecules to the binding site of hERRγ. During docking, the initial structure and coordinate of the complex were obtained by retaining crystal water. Docking between ligands, BPF and BP(2,2)(Un), and hERRγ was conducted by AutoDockTools graphical user interface. We applied the semi-flexible docking approach, maintaining the rigidity of hERRγ while allowing flexibility in these three EDCs. The grid box was defined according the 4-isopropylphenol binding pocket. The grid center coordinates on hERRγ were defined as − 15.28, Y − 5.15, and − 28.06 in the *X*, *Y*, and *Z* directions. The grid size was set as 60 Å × 60 Å × 60 Å, and spacing between the grid points was 0.375 Å. Docking was performed with Lamarckian genetic algorithm and default parameters. And then, the strongest binding mode was retained for further analysis according to the molecular docking mode. Lack hydrogen atoms were then appended applying tLeap program in

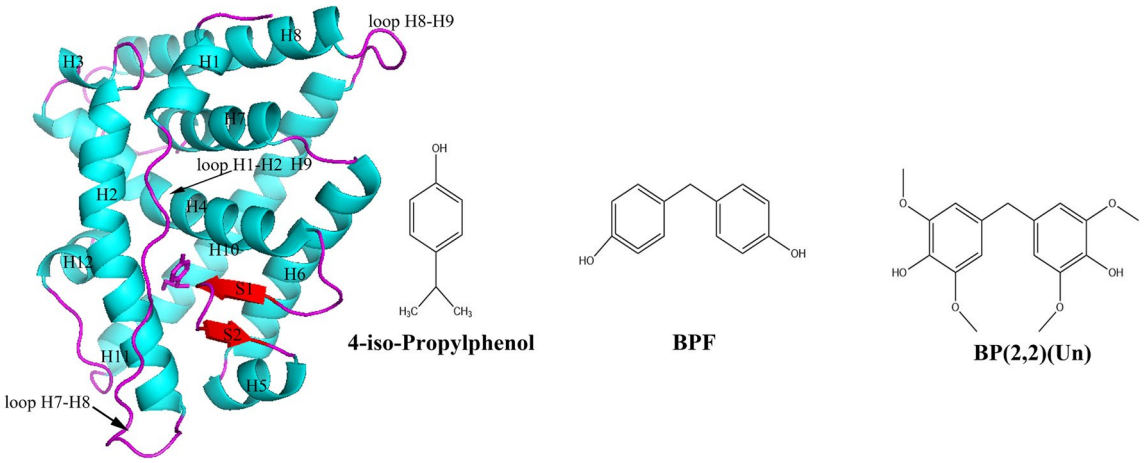

Fig. 1 Cartoon structure of hERRγ-4-isopropylphenol complex (**A**, PDB ID: 6I65) and molecular structures of three EDCs (**B**)

Amber 18 [28]. Standard Amber ff14SB force filed [29] and general amber force filed [30] plus AM1-BCC charges were performed to form force field parameters of hERRγ and these EDCs, respectively. Antechamber program in Amber was used to assign appropriate force field atom types for these three EDCs. Truncated octahedral periodic box composing TIP3P water [31] was placed into each system. At the same time, distance of water box with outermost atoms was ensure to be no less than 12 Å. Overall, each system included over 12,000 water molecules, and the volumes of the solvated box are about 410,000 $Å^3$. Besides, to stay neutrality, 12 Na^+ was affiliated to each system using the tLeap procedure according to the Coulomb potential grid.

MD simulation

In order to do away with adverse interaction between atoms, firstly, the systems underwent steepest descent of 4000 steps and conjugate gradients of 8000 steps under 50 kcal mol^{-1} $Å^{-2}$ constraint. Subsequently, they were further minimized in 8000 steps with all atoms unrestricted. After minimization, applying harmonic restraints with 10 kcal mol^{-1} $Å^{-2}$ force constants on the solute atoms, the temperature was progressively increased to 310 K in 600 ps, then an equilibrium process of 1000 ps. As can be seen from the plots of energy, temperature, and pressure (Fig. S2), clearly, during equilibrium, all complexes showed high stability. Finally, three repeated 250 ns simulations for each system were eventually conducted under *NPT* ensemble using periodic boundary conditions. Randomly assign three seeds with different values to repeated system according to Maxwell's distribution. The system temperature was kept at 310 K by coupling to a Langevin heatbath with a collision frequency of 1 ps^{-1}, while maintaining a constant isotropic pressure at 1 bar using the Berendsen barostat. The time step was set to 2 fs. Particle mesh Ewald method [32] to handle remote electrostatic interactions was conducted. SHAKE algorithm [33] dealt with bonds associating hydrogen atoms. Coordinate trajectories were recorded every 2 ps for subsequent analysis. Hydrogen bonds are considered when the distance between the donor and acceptor is less than 3.5 Å and the angle formed is less than 120°. Electrostatic interactions are considered when the distance is below 4.5 Å. For the hydrophobic interactions, functional groups with a distance shorted than 5.0 Å are taken into account. Data analysis was mainly carried out by cpptraj program in Amber. The PyMOL software [34] was utilized to visualize the trajectories and create structural representations.

MM-PBSA calculation

We extracted 3000 snapshots from the equilibrated portions at 200-ps intervals for energy calculations (ΔG_{bind}) by MM-PBSA method [35–39] using single trajectory in amber. ΔG_{bind} of these EDCs (G_{ligand}) binding to hERRγ (G_{receptor}) to yield the complex ($\Delta G_{\text{complex}}$) is broken down into distinct energy items as follows:

$$\Delta G_{bind} = G_{complex} - G_{receptor} - G_{ligand} \quad (1)$$

$$\Delta G_{bind} = \Delta H - \Delta S \quad (2)$$

$$\Delta H = \Delta E_{ele} + \Delta E_{vdW} + \Delta G_{PB} + \Delta G_{SA} \quad (3)$$

$$\Delta G_{SA} = \gamma \Delta SASA + \beta \quad (4)$$

Enthalpy (ΔH) includes electrostatic interaction energy (ΔE_{ele}), van der Waals interaction energy (ΔE_{vdW}), polar solvation energy (ΔG_{PB}), and nonpolar solvation energy

(ΔG_{SA}). ΔG_{PB} is estimated using PB model, and ΔG_{SA} is calculated by solvent accessible surface area (ΔSASA). γ and β in the formula are 0.00542 kcal mol^{-1} Å^{-2} and 0.92 kcal mol^{-1}, respectively. In addition, the ionic strength was 0.1 M. Dielectric constants of solute and solvent were 2.0 and 80.0, respectively [40]. Conformations entropy change ($T\Delta S$) is usually computed using Normal-mode analysis [41]. Considering computational cost, entropy is calculated based on the equilibrated trajectories by extracting 100 snapshots at 6-ns intervals.

Apart from conducting binding free energy calculations, the molecular mechanics/generalized born surface area (MM-GBSA) energy decomposition method was conducted by taking into account molecular mechanics and desolvation energies without accounting for entropy contributions.

$$\Delta G_{bind}(\rho, D_{in}, \alpha, \gamma, C) = \alpha[E_{Coul}(D_{in}) + E_{vdw} + \Delta G_R(\rho, D_{in}) + G_{cav}(\rho) + C] \quad (5)$$

$$G_{cav} = \gamma \Delta M_{SA} \quad (6)$$

ΔG_{bind} includes intermolecular Coulomb energy (E_{Coul}), van der Waals (E_{vdW}), reaction energy (ΔG^R), and nonpolar solvation energy (G_{cav}). ΔG^R and G_{cav} were computed based on boundary element method and solvent-accessible surface area (ΔMSA), respectively.

The parameters of ρ (linear scaling factor of van der Waals radii), D_{in} (internal dielectric invariable of solute), α, γ, and C are obtained according to energy values measured in experiment and were 1.1, 2.25, 0.1048, 0.0129 kcal mol^{-1} Å^{-2}, and − 2.89 kcal mol^{-1}, respectively.

Conformational dynamics analysis

To intuitively observe internal structure changes of hERRγ induced by different EDCs, cross-correlation matrix (C_{ij}) was performed [43] as follows:

$$C_{ij} = \frac{< \Delta r_i \Delta r_j >}{(< \Delta r_i^2 >< \Delta r_j^2 >)^2} \quad (7)$$

The sharp brackets and Δr_i represent the mean simulation time and displacement from mean position of ith atom, respectively. The C_{ij} values are taken from − 1 to 1. If C_{ij} is greater than zero, it means that atoms i and j are positively correlated; otherwise, it shows that atoms i and j are negatively correlated.

Principal component analysis

To reveal motion changes of functional significance, principal component analysis (PCA) [44–46] was conducted. To scrutinize the impact of each residue, the total energy between hERRγ and EDCs was dissected into individual residues to pinpoint the key residues involved in the interaction with these EDCs.

SIE calculation

The energy between EDCs and hERRγ (ΔG_{bind}) was also calculated with the *sietraj* program, which employed the SIE method for computation [25, 26, 42]. The same 3000 snapshots at 200-ps intervals as MM-PBSA methods were performed for SIE calculations. The SIE function utilizes the following physical parameter dependencies as outlined below:

Based on ProDy software [47], according to the sampling from the joined equilibrated trajectories, covariance matrix of diagonal coordinate system is constructed by PCA, and the movement of hERRγ can be observed as follows: (a) project trajectories through direction depicted by corresponding eigenvector, (b) compute the first two eigenvalues, thus determining the highest directions of hERRγ. Three-dimensional structure snapshots of hERRγ were visualized by VMD [48] software with its plug-in NMWiz.

Results and discussion

MD simulation analysis

To insight into overall structural stability, root mean square deviations (RMSDs) of these complexes were measured (Fig. S3). Obviously, all complexes showed high stability fluctuation around 2.2 Å in the last 200 ns time of each simulation. The stability of the simulated trajectory can also be demonstrated from the evolution of the rotation radius, SASA, and hydrogen bond over time in Fig. S4. Thus, the following analysis was carried out for equilibrated 600 ns trajectories after stabilization. For complexes of hERRγ and 4-isopropylphenol, BPF, BP(2,2)(Un), and RMSD values are 2.35, 2.13, and 1.98 Å, respectively. Clearly, during simulations, hERRγ in three complexes did not experience primary structural transformation, which is compatible with the outcome of experimental by Thouennon et al. [12] and can also be observed in Figs. S5 and S6. All simulated hERRγ-EDC complexes converged and displayed stable trajectories, validating the stability of these hERRγ-EDC complexes and also confirming the applicability of simulation methods for them. Moreover, by selecting structures from the simulations

and calculating enthalpy and entropy values, stability of simulated trajectory can be further inferred (Figs. S7 and S8). Although enthalpy and entropy reckoned for various snapshots are quite different, their cumulative mean became stable expeditiously within equilibrated 600 ns trajectory. It leads to conclude equilibrated 600 ns trajectory should be rational and trustworthy for subsequent analysis.

For investigating the reason for difference of structure and flexibility of hERRγ when binding with EDCs, root mean square fluctuations (RMSF) was calculated (Fig. S9). On the whole, RMSF values of hERRγ varied similarly across the studied systems, except for variations in individual regions. Most varied residues are in the N-terminal, C-terminal, and loops in hERRγ, and residues in β-sheets S1 and S2 varied as well. Whereas for these complexes, residues near the active pockets have lower values, indicating hydrophobic binding pockets formed in the above regions maintain strong stability during simulations. Interestingly, among all these complexes, loops H1-H2, S1-S2, H7-H9, and H11-H12 showed distinct flexibility. What's more, to investigate movements of different regions for hERRγ when binding to distinct EDCs, correlated fluctuations of Cα were reckoned (Fig. S10). Among these complexes, internal motions in domains D1 among H2 with H3-H4, D2 among H2 with s1, s2, as well as H5, D3 among H3-H4 with H7-H8, D4 among H4-H5 with H5-H7, D5 among H5-H6 with H10-H12, and D6 among H7-H8 with H8-H9 were more obvious changes. It can be seen that the above deviations for internal dynamics of hERRγ corresponded to the relative position changes of residues when binding to various EDCs, thus leading to changes in their binding affinity.

Binding free energy analysis

To describe differences in the interactions of various EDCs with hERRγ, MM-PBSA was first applied to reckon different energy terms (Table 1). Binding free energies between 4-isopropylphenol, BPF and hERRγ are − 5.39 and − 5.16 kcal/mol, respectively. The order of energy calculation was in accordance with experimental consequence for hERRγ-4-isopropylphenol (− 8.89 kcal/mol) and hERRγ-BPF (− 8.44) complexes [12]. After calculating energy errors, the order of energy results was still the same as that of removing the errors. Moreover, binding free energy were − 4.84 kcal/mol for hERRγ-BP(2,2)(Un) complex, which has a similar trend to ERα [17]. The differences between the energy obtained by MM-PBSA method and the experimental results are mainly caused by the following aspects [35, 36, 39, 40]: (1) variations in the dielectric constant ε across protein internal residues are not considered in MM-PBSA calculations; (2) the discrepancy in water models used between MM-PBSA calculations (implicit solvent) and MD simulations (explicit solvent); (3) the limited sampling of conformational entropy due to computational constraints can hinder direct comparisons with experimental data; and (4) energy calculations based on initial structures instead of multiple MD snapshots reduce computational time but overlook dynamic effects, leading to predictions heavily reliant on initial structures and lacking statistical accuracy information. Nevertheless, the MM-PBSA method provides a reliable ranking of energies across various systems, demonstrating a strong correlation with experimental findings. In analysis of composition of these various complexes, nonpolar energy, particularly van der Waals, acts as primary driving force for EDCs interacting with hERRγ. The hERRγ-BP(2,2)(Un) complex showed the highest van der Waals energy (− 46.30 kcal/mol), whereas hERRγ-4-isopropylphenol and hERRγ-BPF complexes are 23.98 and 20.02 kcal/mol lower than that of hERRγ-BP(2,2)(Un). At the same time, electrostatic interaction energy of these complexes also afforded beneficial contributions. When interacting with hERRγ, BPF brought out superior electrostatic interaction energy (− 22.66 kcal/mol) than 4-isopropylphenol (− 14.81 kcal/mol) and BP(2,2)(Un) (− 5.49 kcal/mol). Among them, electrostatic interaction energies of BP(2,2)(Un) interacting with hERRγ w oppositely minor. The above results were consistent with the following analysis about hydrogen bonds. Electrostatic solvation interactions generated by various EDCs with hERRγ disrupt their binding, whereas nonpolar solvation interactions showed opposite trend. For entropy in hERRγ-4-isopropylphenol, hERRγ-BPF, and hERRγ-BP(2,2)(Un) complexes are 14.65, 14.86, and 22.19 kcal/mol, respectively. These discrepancies were chiefly caused by vibrational entropy, which was related to structural transformation of hERRγ interacting with various EDCs. For the

Table 1 Binding free energy and its terms (kcal/mol) of EDCs-hERRγ complexes by MM-PBSA

System	hERRγ-4-iso	hERRγ-BPF	hERRγ-BPUn
ΔE_{vdW}	− 22.32 ± 2.12	− 26.28 ± 2.47	− 46.30 ± 2.71
ΔE_{ele}	− 14.81 ± 2.20	− 22.66 ± 4.09	− 5.49 ± 3.34
$\Delta E_{(MM)}$	− 37.13 ± 2.16	− 48.94 ± 3.38	− 51.79 ± 3.04
ΔG_{PB}	18.50 ± 1.79	30.97 ± 2.89	28.12 ± 2.97
ΔG_{SA}	− 1.41 ± 0.07	− 2.05 ± 0.09	− 3.36 ± 0.12
ΔG_{sol}	17.09 ± 1.27	28.92 ± 2.04	24.76 ± 2.10
ΔG_{polar}	3.69 ± 2.00	8.31 ± 3.54	22.63 ± 3.16
ΔG_{nonpol}	− 23.73 ± 0.15	− 28.33 ± 1.75	− 49.66 ± 1.92
ΔH	− 20.04 ± 3.85	− 20.02 ± 3.85	− 27.03 ± 3.69
-TΔS	14.65 ± 2.97	14.86 ± 3.97	22.19 ± 2.38
ΔG_{bind}	− 5.39 ± 3.43	− 5.16 ± 3.52	− 4.84 ± 3.10
ΔG_{exp}	− 8.89	− 8.44	

Data is presented as value ± standard deviation. $\Delta H = \Delta G_{polar} + \Delta G_{nonpol} = \Delta E_{ele} + \Delta G_{PB} + \Delta E_{vdW} + \Delta G_{SA}$. Experimental energies (ΔG_{exp}) were reckoned by inhibition constants (K_i) based on $\Delta G_{exp} = RT\ln K_i$

hERRγ-BP(2,2)(Un) complex, the increase in conformational entropy is mainly due to the expansion of hydrophobic side chain size through the two methoxy substituents, and the increase in steric hindrance around the binding pocket leads to the structural instability of the complex. This should be one of the reasons for their weakened energy.

To verify the above energy results, SIE approach was also performed to assess their binding energy (Table 2). Energies between hERRγ and 4-isopropylphenol, BPF, and BP(2,2)(Un) are − 6.30, − 6.23, and − 5.93 kcal/mol, respectively. The energy order was also consistent with experimental measurements [12, 17]. By analyzing the results obtained by both calculation methods, we believed that they are used trustworthy to further explore the interactional ways of EDCs with hERRγ. In analyzing various energy terms, nonpolar interactions (ΔG_{nonpol}), including ΔE_{vdW} and nonpolar contributions (ΔG_{cav}) play positive role in interactions between these EDCs and hERRγ. Therefore, hydrophobic interaction was the major driving force for these EDCs interacting with hERRγ. What's more, ΔE_{vdW}, ΔE_{Coul}, and ΔG_{cav} played the active role in their binding. ΔG^{R} (reaction energies) are between 5.26 and 9.30 kcal/mol, which are not conductive to interact between various EDCs and hERRγ. Despited ΔE_{Coul} also generated an active function on the binding of EDCs to hERRγ; this effect was offseted by ΔG^{R}. To sum up, hydrophobic interactions consisting mainly of van der Waals energies play a crucial role in stabilization of the EDCs-hERRγ complexes. Results of the above analysis were consistent with our preceding MM-PBSA analysis and experimental measurements [12, 17].

Table 2 Binding free energy and its terms (kcal/mol) of EDCs-hERRγ complexes by SIE

System	hERRγ-4-iso	hERRγ-BPF	hERRγ-BPUn
ΔE_{vdW}	− 25.06 ± 2.04	− 26.16 ± 2.69	− 27.98 ± 2.74
ΔE_{Coul}	− 7.62 ± 1.04	− 7.32 ± 1.97	− 5.21 ± 1.76
ΔG_{cav}	− 5.15 ± 0.22	− 6.53 ± 0.27	− 5.18 ± 0.36
ΔG^{R}	5.26 ± 0.51	8.15 ± 0.99	9.30 ± 1.2
ΔG_{nonpol}	− 30.21 ± 0.82	− 32.69 ± 1.56	− 33.16 ± 1.51
ΔG_{pol}	− 2.36 ± 1.45	0.83 ± 1.91	4.09 ± 1.95
ΔG_{bind}	− 6.30 ± 0.16	− 6.23 ± 0.25	− 5.93 ± 0.34
ΔG_{exp}	− 8.89	− 8.44	

Data is presented as value ± standard deviation. $\Delta G_{pol} = \Delta G^{R} + \Delta E_{Coul}$, $\Delta G_{nonpol} = \Delta G_{cav} + \Delta E_{vdw}$. Experimental energies (ΔG_{exp}) were reckoned by inhibition constants (K_i) based on $\Delta G_{exp} = RT\ln K_i$

Key residues in stabilizing complexes

For investigating hotspots of hERRγ binding to EDCs, interactions between these three EDCs and residues were analyzed. The key residues, identified based on a contribution exceeding − 0.5 kcal/mol, are shown in Fig. 2 and listed in Tables S1–S3. In short, four regions near L271, L309, L345, as well as F435 played main roles in interacting with various EDCs. Hydrophobic residues are key residues that mainly affected the binding of various EDCs to hERRγ such as leucine. And they are almost verified by static structures from experiment [7]. For instance, with 4-isopropylphenol, residues E275, and R316 formed hydrogen bonds, while F435 formed C–H-π interactions. Almost all key residues binding with EDCs obviously possessed smaller polar interactions and somewhat larger non-polar interactions (Tables S1–S3 and Fig. 3). As bound to various EDCs, in addition to residue E275, a good many of residues that took part in polar interactions are involved in hydrogen bonds (Fig. 4 and Table S4), which were not listed when the probability is small.

In light of Fig. 2A and Table S1, interactions between 4-isopropylphenol and ten residues are greater than − 0.5 kcal/mol. Remarkably, resides L271, A272, E275, L309, and V313 contributed more than − 1 kcal/mol. In the study of nonpolar interactions in hERRγ-4-isopropylphenol complex (Fig. 3A), we found that five residues, including L268, L271, A272, L309, and Y326, had energies above − 1 kcal/mol. While studying polar interaction (Fig. 3A), there is only one critical residue, E275, whose energy is above − 1 kcal/mol, as well as their distributions were shown (Fig. 4A). Energies of residues L268, L271, A272, and V313 with 4-isopropylphenol are − 0.98, − 1.37, − 1.16, and − 1.06 kcal/mol, respectively.

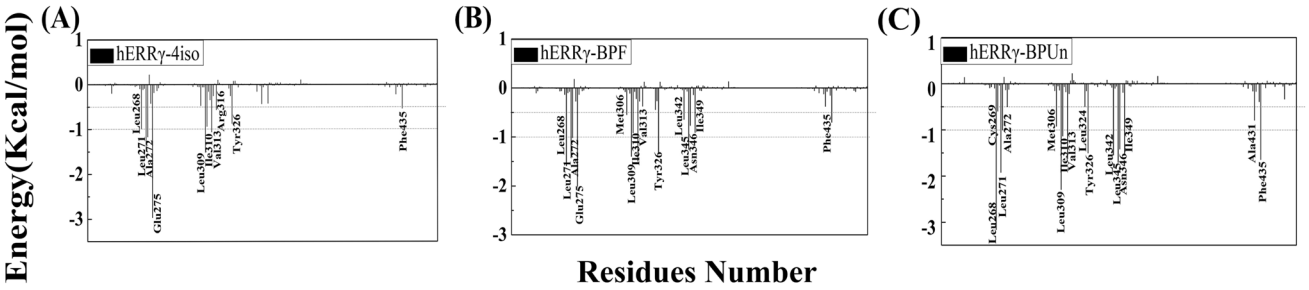

Fig. 2 Important residues contributions for different complexes. A hERRγ-4-isopropylphenol. **B** hERRγ-BPF. **C** hERRγ-BP(2,2)(Un)

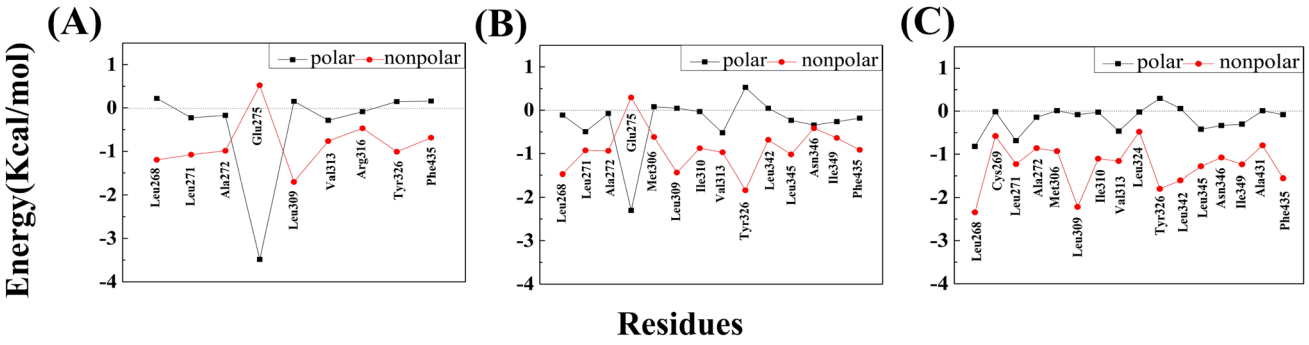

Fig. 3 Nonpolar interaction and polar interaction energy for key residues. **A** hERRγ-4-isopropylphenol. **B** hERRγ-BPF. **C** hERRγ-BP(2,2)(Un)

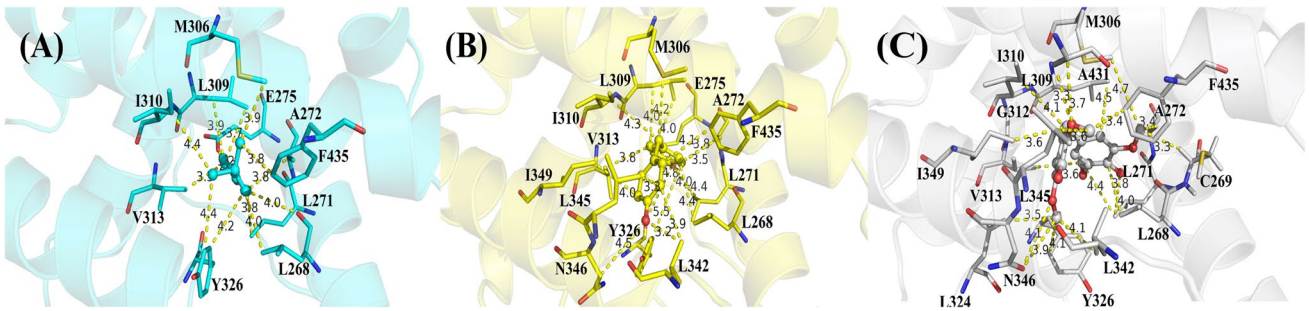

Fig. 4 Interactions between various EDCs and hERRγ. **A** hERRγ-4-isopropylphenol. **B** hERRγ-BPF. **C** hERRγ-BP(2,2)(Un)

They are consistent with the interaction of their hydrophobic alkyls with benzene group of 4-isopropylphenol. The isobutyl-methyl group of L309 and benzene group of Y326 in CH-π and T-shaped π-π interactions with 4-isopropylphenol contributing energies with − 1.51 and − 0.87 kcal/mol, respectively. The alkyl of I310 and alkyl group of 4-isopropylphenol produces − 0.93 kcal/mol energy. And interaction of van der Waals (− 0.60 kcal/mol) between F435 and side chain of 4-isopropylphenol is one of the essential causes for changing in energy (Fig. 4A). Interaction between L309 and 4-isopropylphenol is about − 1.51 kcal/mol. It related with interaction of CH-π formed by hydrophobic alkyl group of L309 with phenol group of 4-isopropylphenol. Hydrophobic interaction formed by benzene ring of F435 with alkyl of 4-isopropylphenol is about − 0.53 kcal/mol. This results from the benzene group of F435 and alkyl group of 4-isopropylphenol. While residue E275 provides − 2.96 kcal/mol energy with 4-isopropylphenol, mainly because the hydrogen bond occupancy of E275-OE1-H···OAC-4-isopropylphenol is about 92.27% (Table S4).

Observing hERRγ-BPF complex, 14 residues contributed more than 0.5 kcal/mol (Fig. 2B). Significantly, residues L268, L271, A272, E275, L309, V313, Y326, together with N345 have a major contribution exceeding − 1 kcal/mol. In accordance with Fig. 3B, the absolute value of four residues L268, L309, Y326, and L345 are greater than − 1 kcal/mol for nonpolar interaction in hERRγ-BPF complex (Tables S2). Besides, polar interaction of residue E275 over − 1 kcal/mol plays an active role in their interaction (Fig. 4B). Residues L271, E275, L309, I310, and F435 have a total energy resembling to that of hERRγ-4-isopropylphenol complex and also play the prominent interaction with BPF. The reason for these residues is similar to the role of them in hERRγ-4-isopropylphenol complex. Compared with hERRγ-4-isopropylphenol complex, energy of L268 is enhanced about 0.61 kcal/mol resulted from enhancing CH-π interaction forming by side chain of L268 with benzene of BPF. Increased interaction of hydrophobic alkyl of V313 and benzene group of BPF results into increased their nonpolar interaction. By comparison to hERRγ-4-isopropylphenol, interaction between alkyl group of A272 and phenol of BPF is reduced approximately 0.15 kcal/mol. It is caused by increased distance between these two groups. Interaction forming by hydrophobic benzene group of Y326 with benzene group of BPF is enhanced about 0.45 kcal/mol. The above outcome is consistent with decreased distance between them. Although BPF is present O–H···O interaction with carbonyl oxygen of Y326, but electrostatic energy in gas phase of Y326 is − 1.48 kcal/mol, this profitable factor is completely shielded by electrostatic energy of liquid phase, thus weakening their interaction. Interaction between I349 and BPF is increased by 0.52 kcal/mol by comparison

to hERRγ-4-isopropylphenol complex. This seemed to be consistent with enhanced interaction between hydrophobic alkyl of I349 and benzene group of BPF. In addition, the oxygen atom of Ala431 and phenolic hydroxyls of BPF also form the hydrogen bond with the occupancy about 67.96; the residue provides about − 0.88 kcal/mol electrostatic energy with BPF. But this profitable factor is completely shielded by electrostatic energy of liquid phase, thus weakening their interaction (Table S4).

In hERRγ-BP(2,2)(Un) complex, 16 residues have energy values over − 0.5 kcal/mol (Fig. 2C). More important, 12 residues L268, L271, A272, L309, I310, V313, Y326, L342, L345, N346, I349, and F435 provide more than − 1 kcal/mol. When dissecting nonpolar interaction in hERRγ-BP(2,2)(Un) complex (Fig. 3C), absolute value of 11 residues, including L268, L271, L309, I310, V313, Y326, L342, L345, L346, I349, and F435, is over 1 kcal/mol (Tables S3 and Fig. 4C). Whereas, nearly all of key residues bound to BP(2,2)(Un) had minor polar interactions. Residues L268, L309, and I349 had a similar variation in total energy as other complexes, and also played important roles in hERRγ-BP(2,2)(Un). Carbonyl oxygen of L268 is nearby hydrophobic methoxyl of BP(2,2)(Un), which tended to form CO-OC interactions. The results showed that contribution of residue L268 to the interaction between BP(2,2)(Un) is − 3.16 kcal/mol. Hydrophobic benzene group of L342 and F435 located close methoxyl group of BP(2,2)(Un), and tend to form π-HC interactions, providing energy nearly − 1.54 and − 1.64 kcal/mol. Leu268, L271, Leu309, V313, L324, Y326, L342, L345, N346, and I349 showed enhanced interaction with BP(2,2)(Un) compared with hERRγ-4-isopropylphenol. It stems from reducing distance forming hydrophobic alkyls of them with methoxyl of BP(2,2)(Un). This suggested that these residues are of great importance in interaction with BP(2,2)(Un). CO-OC interactions is also found between arbonyl oxygen of N346 and hydrophobic methoxy group of BP(2,2)(Un), and thus electrostatic energy (− 0.68 kcal/mol) is the chief driving force. Overall, hydrophobic methoxide groups are the primary cause for the energy distinction of above pivotal residues. Two methoxy substituents ortho to the hydroxyl group enlarges the size of the hydrophobic side chain through the methoxy groups, and this effect may be due to an increase in steric hindrance around the binding pocket. This steric hindrance weakens the hydrogen bonds between BP(2,2)(Un) and several important residues such as Glu275, Tyr316, and Ala431, thereby reducing the binding of these phenolic hydroxyl groups to hERRγ, which should be one of the reasons for their weakened energy.

Based on the above analysis, we can infer these EDCs lead to local structure changes in loops H1-H2, H7-H8, together with H8-H9 mainly by influencing their interactions with various residues, which can be confirmed by the most representative structural superimposition in Figs. S11 and S12. Residues near L268, V313, L345, and F435 can stably bind to these EDCs, in which CH-π, π-π, and hydrogen bonds interactions are the key roles of these EDCs with important residues of hERRγ.

Conclusion

In this study, molecular docking, MD simulations with MM-PBSA, and SIE means were conducted to uncover conformational change and interaction of these three EDCs with hERRγ. When various EDCs bind to hERRγ, domains near residues L268, V313, L345, and F435 contribute significantly to the interaction of these hERRγ-EDCs complexes. And hydrophobic interactions consisting mainly of van der Waals energies play a crucial role in stabilization between them, which were essential for their interacting. What's more, interactions of CH-π, π-π, and hydrogen bonds are essential in stabilization of EDCs with hERRγ. And most noticeable of all, the binding of the hydrophobic methoxide groups of BP(2,2)(Un) is useful for decreasing the binding ability between EDCs and hERRγ. The structural and energy information uncovered in our study can provide estimable knowledge for the search for further insights into the effects of EDCs on health problems.

Supplementary Information The online version contains supplementary material available at https://doi.org/10.1007/s00894-024-05926-z.

Author contributions Lin Chen contributed to the conception of the study and wrote the manuscript; Ying Sun performed the experiment and manuscript preparation; Bing Zhao helped perform the analysis with constructive discussions; Ruige Wang performed the data analyses and wrote the manuscript.

Funding This work was supported by Fundamental Research Funds for Heilongjiang Educational Committee of Chinese hemp specialty (145209504).

Data availability The datasets can be obtained from the corresponding author, through email request, reasonable request.

Declarations

Ethical approval Not applicable.

Consent to participate Not applicable.

Consent for publication Not applicable.

Competing interests The authors declare no competing interests.

References

1. Mushtaq N, Singh DV, Bhat RA, Dervash MA, Hameed OB (2020) Freshwater contamination: sources and hazards to aquatic biota. Freshw Pollut Dynamics Remediation 27–50. https://doi.org/10.1007/978-981-13-8277-2_3
2. van Wezel AP, van den Hurk F, Sjerps RM, Meijers EM, Roex EW, Ter Laak TL (2018) Impact of industrial waste water

treatment plants on Dutch surface waters and drinking water sources. Sci Total Environ 640:1489–1499
3. Yilmaz B, Terekeci H, Sandal S, Kelestimur F (2020) Endocrine disrupting chemicals: exposure, effects on human health, mechanism of action, models for testing and strategies for prevention. Rev Endocr Metab Dis 21:127–147
4. Sifakis S, Androutsopoulos VP, Tsatsakis AM, Spandidos DA (2017) Human exposure to endocrine disrupting chemicals: effects on the male and female reproductive systems. Environ Toxicol Phar 51:56–70
5. Giulivo M, de Alda ML, Capri E, Barceló D (2016) Human exposure to endocrine disrupting compounds: their role in reproductive systems, metabolic syndrome and breast cancer. A review. Environ Res 151:251–264
6. Thompson DC, Perera K, London R (1995) Quinone methide formation from para isomers of methylphenol (cresol), ethylphenol, and isopropylphenol: relationship to toxicity. Chem Res toxicol 8(1):55–60
7. Usman A, Ikhlas S, Ahmad M (2019) Occurrence, toxicity and endocrine disrupting potential of bisphenol-B and bisphenol-F: a mini-review. Toxicol Lett 312:222–227
8. Heard DJ, Norby PL, Holloway J, Vissing H (2000) Human ERRγ, a third member of the estrogen receptor-related receptor (ERR) subfamily of orphan nuclear receptors: tissue-specific isoforms are expressed during development and in the adult. Mol Endocrinol 14(3):382–392
9. Huss JM, Garbacz WG, Xie W (2015) Constitutive activities of estrogen-related receptors: transcriptional regulation of metabolism by the ERR pathways in health and disease. Biochimica et Biophysica Acta (BBA)-Molecular Basis of Disease 1852(9):1912–1927
10. Miki K, Deguchi K, Nakanishi-Koakutsu M, Lucena-Cacace A, Kondo S, Fujiwara Y, Hatani T, Sasaki M, Naka Y, Okubo C, Narita M, Takei I, Napier SC, Sugo T, Imaichi S, Monjo T, Ando T, Tamura N, Imahashi K, Nishimoto T, Yoshida Y (2021) ERRγ enhances cardiac maturation with T-tubule formation in human iPSC-derived cardiomyocytes. Nat Commun 12(1):3596
11. Matsushima A, Kakuta Y, Teramoto T, Koshiba T, Liu X, Okada H, Tokunaga T, Kawabata S, Kimura M, Shimohigashi Y (2007) Structural evidence for endocrine disruptor bisphenol A binding to human nuclear receptor ERRγ. J Biochem 142(4):517–524
12. Thouennon E, Delfosse V, Bailly R, Blanc P, Boulahtouf A, Grimaldi M, Balaguer P (2019) Insights into the activation mechanism of human estrogen-related receptor γ by environmental endocrine disruptors. Cell Mol Life Sci 76:4769–4781
13. Audet-Walsh É, Yee T, McGuirk S, Vernier M, Ouellet C, St-Pierre J, Giguere V (2017) Androgen-dependent repression of ERRγ reprograms metabolism in prostate cancer role of ERRγ in prostate cancer cell metabolism. Cancer Res 77:378–389
14. Madhavan S, Gusev Y, Singh S, Riggins RB (2015) ERRγ target genes are poor prognostic factors in tamoxifen-treated breast cancer. J Exp Clin Canc Res 34:1–8
15. Fujimura T, Takahashi S, Urano T, Ijichi N, Ikeda K, Kumagai J, Mursta T, Takayama K, Horie-inoue K, Ouchi Y, Muramatsu M, Inoue S (2010) Differential expression of estrogen-related receptors β and γ (ERRβ and ERRγ) and their clinical significance in human prostate cancer. Cancer Sci 101:646–651
16. Legler J, Fletcher T, Govarts E, Porta M, Blumberg B, Heindel JJ, Trasande L (2015) Obesity, diabetes, and associated costs of exposure to endocrine-disrupting chemicals in the European Union. J Clin Endocrinol Metab 100:1278–1288
17. Amitrano A, Mahajan JS, Korley LT, Epps TH (2021) Estrogenic activity of lignin-derivable alternatives to bisphenol A assessed via molecular docking simulations. RSC Adv 11:22149–22158
18. Xue Q, Liu X, Liu XC, Pan WX, Fu JJ, Zhang AQ (2019) The effect of structural diversity on ligand specificity and resulting signaling differences of estrogen receptor α. Chem Res Toxicol 32:1002–1013
19. Li L, Wang Q, Zhang Y, Niu Y, Yao X, Liu H (2015) The molecular mechanism of bisphenol A (BPA) as an endocrine disruptor by interacting with nuclear receptors: insights from molecular dynamics (MD) simulations. PLoS ONE 10:e0120330
20. Sharma J, Bhardwaj VK, Das P, Purohit R (2021) Identification of naturally originated molecules as γ-aminobutyric acid receptor antagonist. J Biomol Struct Dyn 39(3):911–922
21. Singh R, Bhardwaj VK, Sharma J, Das P, Purohit R (2022) Identification of selective cyclin-dependent kinase 2 inhibitor from the library of pyrrolone-fused benzosuberene compounds: an in silico exploration. J Biomol Struct Dyn 40(17):7693–7701
22. Kumar S, Sinha K, Sharma R, Purohit R, Padwad Y (2019) Phloretin and phloridzin improve insulin sensitivity and enhance glucose uptake by subverting PPARγ/Cdk5 interaction in differentiated adipocytes. Exp Cell Res 383(1):111480
23. Chen L, Huang X, Li Y, Zhao B, Liang M, Wang R (2023) Structural and energetic basis of interaction between human estrogen-related receptor γ and environmental endocrine disruptors from multiple molecular dynamics simulations and free energy predictions. J Hazard Mater 443:130174
24. Na L, Zhou W, Yue G, Wang J, Fu W, Sun H, Li D, Duan M, Hou T (2018) Molecular dynamics simulations revealed the regulation of ligands to the interactions between androgen receptor and its coactivator. J Chem Inf Model 58:1652–1661
25. Sulea T, Cui Q, Purisima EO (2011) Solvated interaction energy (SIE) for scoring protein–ligand binding affinities. 2. Benchmark in the CSAR-2010 scoring exercise. J Chem Inf Model 51:2066–2081
26. Naïm M, Bhat S, Rankin K, Dennis S, Chowdhury S, Siddiqi I, Drabik P, Sulea T, Bayly C, Jakalian A, Purisima E (2007) Solvated interaction energy (SIE) for scoring protein−ligand binding affinities. 1. Exploring the parameter space. J Chem Inf Model 47:122–133
27. Morris GM, Huey R, Lindstrom W, Sanner MF, Belew RK, Goodsell DS, Olson AJ (2009) AutoDock4 and AutoDockTools4: automated docking with selective receptor flexibility. J Comput Chem 30:2785–2791
28. Case DA, Cheatham TE III, Darden TA, Glhike H, Luo R, Merz KM, Onufriev A, Simmerling CL, Wang B, Woods RJ (2005) The amber biomolecular simualtion programs. J Comput Chem 26:1668–1688
29. Maier JA, Martinez C, Kasavajhala K, Wickstrom L, Hauser KE, Simmerling C (2015) ff14SB: improving the accuracy of protein side chain and backbone parameters from ff99SB. J Chem Theory Comput 11:3696–3713
30. Wang J, Wolf RM, Caldwell JW, Kollman PA, Case DA (2004) Development and testing of a general amber force field. J Comput Phys 25:1157–1174
31. Jorgensen WL, Chandrasekhar J, Madura JD, Impey RW, Klein ML (1983) Comparison of simple potential functions for simulating liquid water. J Comput Phys 79:926–935
32. Darden T, York D, Pedersen L (1993) Particle mesh Ewald: an N.log (N) method for Ewald sums in large systems. J Comput Phys 98:10089–10092
33. KrUtler V, Gunsteren WFV, Hünenberger HP (2015) A fast shake algorithm to solve distance constraint equations for small molecules in molecular dynamics simulations. J Comput Chem 22:501–508
34. DeLano WL (2002) Pymol: an open-source molecular graphics tool. CCP4 Newsl Protein Crystallogr 40(1):82–92
35. Hou T, Wang J, Wang Y, Li W (2011) Assessing the performance of the MM/PBSA and MM/GBSA methods. 1. The accuracy of binding free energy calculations based on molecular dynamics simulations. J Chem Inf Model 51:69–82

36. Sun H, Li Y, Tian S, Xu L, Hou T (2014) Assessing the performance of MM/PBSA and MM/GBSA methods. 4. Accuracies of MM/PBSA and MM/GBSA methodologies evaluated by various simulation protocols using PDB bind data set. Phys Chem Chem Phys 16:16719–16729
37. Swanson JM, Henchman RH, McCammon JA (2004) Revisiting free energy calculations: a theoretical connection to MM/PBSA and direct calculation of the association free energy. Biophys J 86:67–74
38. Luo R, David L, Gilson MK (2002) Accelerated Poisson-Boltzmann calculations for static and dynamic systems. J Comput Chem 23:1244–1253
39. Genheden S, Ryde U (2015) The MM/PBSA and MM/GBSA methods to estimate ligand-binding affinities. Expert Opin Drug Dis 10(5):449–461
40. Sun H, Li Y, Shen M, Tian S, Xu PP, Guan Y, Hou T (2014) Assessing the performance of MM/PBSA and MM/GBSA methods. 5. Improved docking performance using high solute dielectric constant MM/GBSA and MM/PBSA rescoring. Phys Chem Chem Phys 16:22035–22045
41. Case DA (1994) Normal mode analysis of protein dynamics. Curr Opin Struc Biol 4:285–290
42. Cui Q, SuleaT SJD, Munger C, Hung MN, Naïm M, Cygler ME, Purisima O (2008) Molecular dynamics-solvated interaction energy studies of protein–protein interactions: the MP1-p14 scaffolding complex. J Mol Biol 379:787–802
43. Hünenberger PH, Mark AE, Van Gunsteren WF (1995) Fluctuation and cross-correlation analysis of protein motions observed in nanosecond molecular dynamics simulations. J Mol Biol 252:492–503
44. Balsera MA, Wriggers W, Oono Y, Schulten K (1996) Principal component analysis and long time protein dynamics. J Phys Chem 100:2567–2572
45. Maisuradze GG, Liwo A, Scheraga HA (2009) Principal component analysis for protein folding dynamics. J Mol Biol 385:312–329
46. David CC, Jacobs DJ (2014) Principal component analysis: a method for determining the essential dynamics of proteins. Protein Dynamics: Methods Protoc 193–226. https://doi.org/10.1007/978-1-62703-658-0_11
47. Bakan A, Meireles LM, Bahar I (2011) ProDy: protein dynamics inferred from theory and experiments. Bioinformatics 27:1575–1577
48. Humphrey W, Dalke A, Schulten K (1996) VMD: visual molecular dynamics. J Mol Grap Model 14:33–38